21 Q*C
10-15-80
2470711 T 15

UCID-18793

NOVA CHAIN DESIGN AND PERFORMANCE

W. W. Simmons,
J. A. Glaze,
J. B. Trenholme,
W. F. Hagen

MASTER

September 4, 1980

Lawrence Livermore Laboratory

Work performed under the auspices of the U.S. Department of Energy by the Lawrence Livermore Laboratory under Contract W-7405-Eng-48.

NOVA CHAIN DESIGN AND PERFORMANCE

W. W. Simmons, J. A. Glaze, J. B. Trenholme, W. F. Hagen
Lawrence Livermore National Laboratory
P. O. Box 5508
Livermore, California 94550

During the past year design of the Nova laser has undergone significant change as a result of developments in our laser glass and optical coating evaluation programs. Two notable aspects of the glass development program deserve emphasis. First, vendor qualification for production of fluorophosphate laser glass is progressing satisfactorily. There is a reasonable expectation that vendors can meet fluorophosphate glass specifications within Nova schedule constraints. Secondly, recent gain saturation measurements have shown that the saturation fluence of the fluorophosphate glass is larger than previously supposed ($\sim$5.5 J/cm^2) and in fact is somewhat larger than Shiva silicate glasses. Hence, performance of Nova for pulses in the 3 ns and longer range should be satisfactory. For pulses in the 1 ns regime, of course, the fluorophosphate chain will have superior performance to that of silicate because of its low nonlinear index of refraction ($\sim$30% that of silicate). These and other considerations have led us to choose a chain design based upon the use of fluorophosphate glass in our amplifiers.

Listed below are several key design and performance features of one baseline Nova chain.

- 9.0 kJ and 9.0 TW at 1 ns
- 11.0 kJ to 13.7 kJ at 3 ns
- 14.0 TW at 100 ps
- Fluorophosphate laser glass
- 460 mm split-disk output amplifier
- 740 mm output and focusing optics
- f/3 final focusing lens

The full Nova system will comprise twenty similar beam lines. Ten of these will be located in the Shiva system bay and ten in the new bay contiguous to Shiva to the east. As will be discussed below, performance per chain may be significantly enhanced over that just quoted.

Nova Design Considerations

Staging: Figure 1 shows an optical schematic of one Nova chain. This chain is comprised of a driver section followed by 315 mm and 460 mm diameter clear aperture output amplifier stages. For the output amplifier stages, each head will hold two disks. The design of these heads will be similar to that of our 340 mm box amplifier. There will be a total of eight disks in the 315 mm stage and six disks in the 460 mm stage. Spacing of the components are such that two additional heads in each stage (dashed figures) could be added should a future upgrade be desirable. Following the last amplifier stage, the beam will be expanded to its full 740 mm final diameter. Final design of the driver section has not yet been completed. However, it will utilize some Shiva amplifiers and spatial filters and may utilize phosphate glass. Between four and five mirrors will route the output beam to the target chamber where it will be focused onto the target with an f/3 lens. Ten such chains will be used in Nova Phase I.

As shown in Figure 1, each chain will be folded at the output of the 208 mm/315 mm spatial filter. With the exception of the oscillator/preamplifier stage, the folded chains including their final spatial filters will be located within the Nova laser bay. All chains will be driven by a common oscillator/preamplifier stage as in Shiva. Tentatively it is planned that the output of this stage will first be split two ways at 50 mm diameter aperture, and then each channel from this division will be split five ways, again at 50 mm diameter aperture. Splitting losses will be recovered through the use of 50 mm rod amplifiers in the two-way and five-way channels. Final decision to drive the Nova chains in this manner has not been made to date. Alternate drive schemes are being evaluated.

The Nova chains will be spatially filtered and fully relayed. The object plane of the relay will be a "hard" aperture placed at the entrance to each chain, with successive image planes occurring at the input lens of each spatial filter/relay element and at the final focusing lens. Figure 2 shows the sizes and spacing of the filter/relay elements. Argus and Shiva elements are also shown for comparison. Table 1 below gives filter/relay parameters for the Nova baseline chain.

The pinhole diameters shown have been chosen so that the beam intensity at the pinhole edge does not exceed 10^{11} W/cm^2 for nominal 10 TW/chain, 1 nsec

performance. Pulses shorter than 1 ns can create larger intensities but will propagate through the pinhole before closure. For longer pulses, the chain B-value decreases, thereby reducing pinhole loading. Calculations of pinhole sizes, of course, depend upon the noise model used. In our calculations we have used a model that has given good agreement with the noise spectrum observed for the Argus and Shiva lasers.

Fluence Limitations: Performance of Nova, as with our other glass laser systems, is limited largely by the threat of beam induced damage to optical components. In the past, the greatest damage threat has been to AR coatings on the input lenses of our spatial filters and on the final focusing lenses. To achieve increased performance from Nova, however, it was advantageous to utilize uncoated filter input lenses but retain the coatings on the SF output lenses and the final focusing lenses. Therefore uncoated as well as AR coated surfaces now pose a potential damage limitation. Coated polarizer and high-reflection surfaces typically have higher thresholds for damage than the AR coated surfaces. Therefore, they do not limit performance for the current Nova design. Bulk damage thresholds are also not anticipated to be a threat.

To assess the threat of surface damage and to develop guidelines for Nova chain design, we evaluated currently available damage data and adopted the following rules.

1) Bulk glass damage and damage to HR coatings are presently not limiting performance.
2) For 1 ns pulses, uncoated surfaces damage at a median fluence of 16 J/cm^2, with 70% of the surfaces tested damaging between 14-19 J/cm^2. At other pulse lengths (0.1 to 3 ns) uncoated surface damage appears to follow a $\sqrt{\tau}$ dependence.
3) Antireflection (AR) surfaces damage at 1 nsec at a median fluence of 5 J/cm^2 with 80% of the surfaces tested damaging between 4-7 J/cm^2. In addition, their damage threshold appears to increase slightly between 1 and 3 nsec and appears to scale as $\sqrt{\tau}$ for pulses shorter than 1 ns.
4) There is a reasonable expectation that damage thresholds will increase. This expectation is based upon recent progress with graded-index AR surfaces, super polish AR coatings and laser polishing of uncoated surfaces.

With these guidelines we established three fluence groups for which to target the Nova design. These groups will hereafter be referred to as the "A", "B", and "C" fluence groups. Figure 3 shows the thresholds for coated and uncoated surfaces in each group. The thresholds in the "A" group represent the median values obtainable today. More specifically, the 1 ns values are the median values obtained by examining a large number of data taken at this pulse length. Other values are then determined using rules 2 and 3 above. Thresholds shown for the "B" group represent the highest values obtainable from today's production coatings and surfaces. Again, values have been scaled from the 1 ns data. The "C" values represent an estimate of what may be possible in the future if one or more of several advanced approaches can be brought to production. Presently, graded-index surfaces look the most promising, with both Corning and Owens Illinois mounting a significant development effort. Less developed are the techniques of laser polishing and super-polishing of substrate surfaces. Research samples have shown that significant increase in damage threshold of a bare surface can be obtained by simply "burnishing" the surface with a directed CO_2 laser beam. In the case of super polish in which the substrate is finished with a bowl-feed process, there is evidence that damage thresholds for AR coatings applied to such surfaces are increased. (Both laser and super polish techniques are presently in a very elemental state and hence should be viewed as a "long shot".)

Perhaps our greatest short-term hope is for graded index parts suitable for damage free laser operation at the "B" fluence levels.

Glass Properties: Choice of fluorophosphate glass for Nova was predicated upon the following considerations: 1) low nonlinear index-of-refraction; 2) saturation fluence parameters competitive with silicate glasses; and 3) reasonable expectation that vendors could deliver this glass to specification. Listed below are some important physical properties of this glass, along with properties of ED-2 silicate glass used extensively in previous systems.

In Table 2 we have shown the lasing wavelength, λ; cross-section for stimulated emission, σ_p; fluorescence lifetime, τ; linewidth, $\Delta\lambda$; linear index-of-refraction, n_0; nonlinear index-of-refraction, n_2; and saturation fluence, E_s. The saturation fluence E_s shown in Table 3 corresponds to a value for which the output fluence from the test sample was 5 J/cm^2.

Recent experiments have shown that saturation fluence parameters are dependent upon the saturating fluence level. This is shown in Figure 4 for the

E-309 glass. In the saturation experiments all test samples were pumped to approximately the same small signal and net gains, so the values shown in Table 2 pro 'de a valid comparison. From all of the data, one concludes that the saturation behavior of fluorophosphate glasses is better than silicate glasses of similar cross-section over the range of fluences tested. The variation of E_s with fluence is accounted for in our performance calculations.

Table 3 below lists specifications on the bulk properties of production fluorophosphate glass. These specifications have been submitted to the three vendors indicated in Table 2. It is currently anticipated that production quality sample disks at 315 mm and 460 mm diameter will be delivered in the Feb-June 1980 time period.

Amplifier Design: New box amplifier designs have been adopted for the 208, 315 and 460 mm aperture disks. The 315 and 208 mm designs will follow from the 340 mm prototype amplifier that has been evaluated over the past year. Both the 315 and 208 mm heads will utilize standard Shiva lamps (44" arc length) that are mounted longitudinally with respect to the axis of the amplifier. The 460 mm head will use short (19" arc length) lamps similar to the lamp used on Shiva rod amplifiers. These will be mounted transverse to the axis of the amplifier; however, other aspects of the design will be similar to the 315 mm head.

Figure 5 shows some important design characteristics of the 315 and 460 mm amplifiers.

Isolation: The power amplifier portion of the Nova chain is protected from self-oscillation by 94 mm, 208 mm and 315 mm diameter Faraday rotators. For the baseline design, the roundtrip small signal gain between the 50 mm Pockel's cell preceding the 94 mm stage and the output of the 460 mm amplifier stage (assuming 100% return) is about 70. Therefore total distributed losses must exceed 98.6% to suppress oscillation. (This loss criterion is not severe. If one imagines, for example, that the loss can be modeled by partially reflecting mirrors placed at each end of that portion of the chain considered above, then the reflectivity of each mirror could be as high as 11.8%.)

However, for the fully expanded chain design, including twelve 315 mm disks and ten 460 mm disks, the margin of safety is small. In this case the roundtrip gain is about 3500 and equivalent mirror reflectivity of less than 1.7%

would be required. A bad AR coating on a PC window, for example, could produce this value. Therefore care must be taken to insure that such surfaces are not aligned normal to the beam line.

Since the last Faraday rotator in the chain is placed at the input to the 315 mm amplifier stage, the Nova chain is particularly vulnerable to light retroreflected from the target. For p-wave polarization at short pulses (small signal gain regime), the returned fluence is amplified by about 150 in passing from the output of the 740 mm spatial filter through the 315 mm amplifier stage. This means that a retroreflection of several percent at the target could, for example, endanger the AR coating on the 315 mm rotator glass. To prevent this, Nova will use a fast triggered plasma shutter to block the pinhole of the last spatial filter. This shutter will produce plasma at the critical density for 1.06 μm light ($\sim 10^{21}$ cm^{-3}) for a time sufficient to absorb light returning from the target or from an opposing amplifier chain.

Nova Performance.

Power and Energy: Figure 6 shows calculated energy and power performance for one baseline Phase I chain. The lower boundaries on the curves are values that can be achieved subject to "A" fluence group limitations. The upper boundaries are values corresponding to "B" fluence group limitations. At "B" levels and long pulses, the curves suggest that performance is limited by gain saturation and energy storage of the amplifiers as much as by damage thresholds. However detailed calculations for pulses longer than 3 ns have not been made. Short pulse performance is limited primarily by small-scale self-focusing effects with concomitant loss at spatial filter pinholes and by growth of spatial filter bandpass modulation over long propagation paths. Additional 315 and 460 mm amplifiers will not significantly contribute to increased performance for either short or long pulses under "B" fluence limitations. Increases in performance for pulses greater than 0.5 ns should be achievable with the addition of amplifiers, however, if damage thresholds can be increased (as, for example, to "C"-fluence limits).

Figures 7, 8 and 9 show MALAPROP calculations of fluence levels throughout the chain for 3 ns, 1 ns and 0.1 ns pulse durations. In these figures the symbol M is used to denote average fluence levels while the solid curves show peak levels of the modulated beam. All calculations were made using the "B"

fluence limitation. At 3 ns this limit was reached at the coated output lens of the 315 mm - 460 mm spatial filter. For long pulses, nonlinear effects become less important and hence the ratio of input to output fluences at the spatial filters approach the geometric expansion ratio. Since this ratio (~2:1) is less than the ratio of coated : uncoated thresholds, the threshold of the coated output lens tends to be the limiting factor for long pulse performance. The "switch over" to the uncoated surface threat appears to be about 1 ns as can be seen in Figure 8. At very short pulses, however, the long propagation path from the output of the last spatial filter to the final focusing lens causes the damage threat to move to the coated surface of this lens as is shown in the 100 ps run of Figure 9. The major contributing factors here are the modulation created by the split disks in the final amplifier and the nonlinear pathlength contribution of the ~50 meter nitrogen/air filled beam tube (see Laser Program Annual Report 1978, Vol. 2, p. 7-99). With nitrogen removed, short pulse damage limit remains at the final focusing lens but, of course, chain output power can be larger.

Figures 10, 11 and 12 show performance curves in relation to respective fluence limits. In Figure 10, the curve labeled "A" represents laser performance obtained with an unmodulated beam of 0.7 fill factor for "A" fluence. The curve labeled "performance" shows computed performance. Separation of the two curves is a measure of peak/average modulation. As the figure shows, the modulation begins to increase rapidly for pulses shorter than 1 ns, but the damage threat remains at the uncoated elements. For pulses longer than 1 ns, beam modulation results largely from linear diffraction and therefore remains relatively constant. Here again the threat is at the coated spatial filter output lenses.

Figure 11 shows the same set of curves for "B" fluence levels. The behavior is qualitatively similar to that of Figure 10, except that for pulses near 1 ns the threatened element shifts to the uncoated SF lenses. Figure 12 shows performance under "C" fluence limitations. Here the nonlinear effects dominate over a much wider range of pulse durations and the damage threat remains at the coated elements throughout the performance range shown. Increase in performance over that obtainable under "B" limitations appears to be modest--ranging from about 6% at 0.1 ns to about 20% at 1 ns and 3 ns. However, values for the "C" limit calculations are based upon extrapolation of "B" limit calculations. Detailed MALAPROP runs have not yet been made.

Short pulse performance (as noted above) for all fluence groups is currently limited by the damage threshold of the final focusing lens. This results from the long propagation path acting on modulation arising from the split disks in the output amplifier. If this threat could be removed by apodization and/or replacement of N_2 with A_r, for example, then the performance would be limited largely by intrastage ΔB considerations. Historically we have limited ΔB to values of about 3.5 because of the appearance of a temporal dip in the output pulse. With a fully relayed chain, the expectation is that increased values of ΔB could be tolerated. This, of course, would lead to improved laser performance. Recently the temporal dip, as observed in early Argus experiments, has been successfully modeled with the MALAPROP code. Similar Nova calculations suggest that, indeed, ΔB's much higher than previously tolerated may well be possible. This is shown in Figure 13 where the threat of damage to the output lens has been removed and MALAPROP calculations performed for "A" and "B" fluences. Also shown is the calculated performance with the traditional ΔB requirement imposed. As observed, these curves suggest that rather impressive performance improvements may be possible with removal of the threat to the output lens.

Long pulse baseline chain performance (for all fluence groups) may actually be better than projected by the MALAPROP code runs to date. The reason is that gain saturation is modeled "globally" by MALAPROP, whereas the real system beam saturates "locally" (i.e., intensity peaks experience less gain than valleys, hence the P/A is reduced relative to that shown in Figure 7, for example). To establish a quantitative handle on this effect, an upgraded version of MALAPROP was implemented, which enabled detailed modeling of gain saturation effects on two-dimensional beams. To illustrate the differences in global and local saturation modeling, in Figure 13A we show anticipated fluences for the Nova baseline chain at 3 ns under both modeling systems (compare the upper curve with Figure 7). It is apparent that the damage threat (to the output lens of the penultimate SF) has been reduced by ~10%. Thus at long pulse durations, there is an additional performance margin (in terms of optical damage threats) relative to that shown, for example, in Figure 11.

Amplified Spontaneous Emission (ASE): Each laser amplifier is a source of fluorescent noise created by spontaneous emission from its inverted population. Additionally, this noise is further amplified by succeeding stages to produce a

net "amplified spontaneous emission" (ASE) from the laser chain. Since much of the ASE arrives at the target before the main irradiating pulse, it represents a damage threat to vulnerable targets.

Figure 14 shows calculated ASE values for the Nova system. Since one option for reducing ASE on Nova is to develop and incorporate a 100 mm diameter Pockels' cell, two sets of calculations are presented: those that assume a 100-mm diameter ASE isolation Pockels' cell placed after the second 100-mm diameter beta amplifier in the chain (in Figure 1 this amplifier is denoted as 9.4 which is the clear aperture (CA) in cm), and those that assume no Pockels' cell in this location. (It is the latter case that we currently consider the baseline design.) Further conditions/assumptions used in the calculations are 1) amplifier gains are chosen to produce peak laser performance at 3 ns (using the notation of previous performance discussions, we denote this as B-fluence limited performance); 2) 100 mm Pockels' cells have a contrast ratio of 30:1; 3) that the amplified fluorescence pulsewidth is 300 μsec at chain output and that the spectral line shape is that given in the LLNL "Laser Glass" handbook; and finally, 4) all Pockels' cell gates are set at 50 ns.

With reference to Figure 14, several broad observations can readily be made. First, the total ASE energy for the baseline system with the PC's closed seems low (5.0 mJ/chain), and that the largest contribution to ASE occurs when the PC's are opened. Second, the ASE energy density on axis and in the focal plane of the final f/3 focusing lens is very large and therefore target surfaces should not be located in this plane. Third, the energy density drops rapidly as one moves away from the focal plane, but is still large (28 J/cm^2) when the PC's are open for 50 ns. And finally, addition of 100-mm Pockels' cells reduces ASE by about X10 when the PC's are closed, but this reduction has a small impact on total ASE accumulated during the gate interval. (Figure 14 shows only the "open gate" values obtained without the 100 mm PC.)

Figure 15 shows the temporal variation of ASE energy density at a location 1 mm forward of the focal plane and total ASE energy for a single chain. Three temporal regions are identified. In region I, the PC's are closed and the ASE increases slowly (150 μsec) to an energy density of 2.5 J/cm^2 and total energy of 2.5 mJ. At this point the PC switches are opened (note temporal scale change) and the ASE values climb rapidly until the switches are closed 50 ns later. Typically, the laser pulse arrives at the center of the PC gate

(here shown at t = 0); so only the additional ASE arising between switch-open and pulse arrival time (region II) is of concern. With the pulse at gate center (t = 0), the ASE values climb to 14 J/cm^2 in density and 12.0 mJ total energy over a time of 25 ns for the baseline (no 100 mm PC) system. While the fluence at this point seems high, the time scale over which it arrives is very short; and therefore it may not represent a damage threat.

Reduction of ASE in region II can be made by moving the pulse arrival time closer to the switch-on time. It is reasonable to expect that, at least for the small PC's in the pre-amp section where much of the ASE originates, this arrival time may be as short as 10 ns. This would reduce ASE to values in the neighborhood of 7 J/cm^2 and 6.0 mJ per chain.

Region III is simply the post shot ASE which appears to be of little consequence with regard to target damage--unless the main pulse fails to be switched out. With our reliable pulse generation systems, this seldom occurs.

Figure 15 shows the spatial distribution of ASE in the focal plane and with the PC's closed. The structure of this "spot" arises because of the changing angular aperture of the spatial filters as one moves from the pre-amp table to final output. Each rectangular portion of this spot reflects the image of an individual spatial filter pinhole. Moving forward of the focal plane, this structure will "wash out"; the spot is then better approximated by a uniform distribution. In arriving at the power and energy densities of Figure 15 and rows 4 and 6 in Figure 14, a uniform distribution was assumed.

We have made estimates of ASE for the baseline fluorophosphate Nova system. These estimates rely largely on the theoretical code calculations of Aaron Budgor, suitably normalized to experimental meaurements on Shiva and to single rod ASE experiments.

Target Irradiation: For Phase I of Nova, each of the ten 740 mm output beams will be focused onto the target with a single element f/3 focusing lens having a focal length of 2.2 meters. The irradiation geometry is that of two opposing clusters of five beams each. Within the limitations of single-beam irregularities ($\pm$ 25%), this allows irradiation of a sphere with the same uniformity as a 12-beam dodecahedral geometry, while maintaining the Argus and Shiva geometry with which we are familiar. The beams in each cluster are arranged as an open cone with a cone angle which can be varied between 80° and 110° by relocating lenses and turning mirrors. Figure 16 depicts the

geometry for a single cluster having a cone angle of 90^0. This figure also shows the five beam composite focal spot size and the image size of the final spatial filter. The focal spot size for an individual beam was estimated at 1 ns using MALAPROP. The composite spot size of 150 μm results when alignment tolerances are included. A peak intensity of about 5×10^{17} W/cm^2 is obtained at 1 ns if all five beams are brought to best focus.

Figure Captions

1) Optical schematic showing one of the Nova amplifier chains. Following the 46 cm amplifier stage, a spatial filter expands the beam to 74 cm diameter for transport to the final target focusing lens. Baseline components are indicated by solid lines. Dashed figures represent later amplifier additions for increased performance.

2) Sizes and spacing of spatial filter/relay elements for Argus, Shiva and Nova. Aperture sizes shown are in cm.

3) Nova design limits for optical damage to antireflection-coated and uncoated optical surfaces.

4) Saturation fluence vs. output fluence from a test sample of E-302 fluorophosphate laser glass. Test data was taken at 1 and 9 ns pulse durations. Center wavelength of the probe pulse was 1.053 μm. The solid curve represents the values that are used in Nova performance simulation codes.

5) Design parameters for Nova 315 and 460 mm power amplifiers.

6) Calculated energy and power performance for the baseline Nova chain. Lower and upper curve boundaries correspond to performance achieved using "A" and "B" damage limits shown in Figure 3.

7) Calculated fluence values along the Nova baseline chain for 3 ns pulses. The solid curve represents peak values of the modulated beam. Average values are denoted by the symbol M. These values are obtained using "B" fluence damage limits shown in Figure 3. Also indicated is that component which first reaches the "B" fluence limit.

8) Calculated fluence values along the Nova baseline chain for 1 ns pulses. The solid curve represents peak values of the modulated beam. Average values are denoted by the symbol M. These values are obtained using "B" fluence damage limits shown in Figure 3. Also indicated is that component which first reaches the "B" fluence limit.

9) Calculated fluence values along the Nova baseline chain for 0.1 ns pulses. The solid curve represents peak values of the modulated beam. Average values are denoted by the symbol M. These values are obtained using "B" fluence damage limits shown in Figure 3. Also indicated is that component which first reaches the "B" fluence limit.

10) Calculated output power and energy for the Nova baseline laser system. The curve labeled "performance" corresponds to calculated values obtained when "A" damage fluence limitations are imposed. The curve labeled "A" corresponds to hypothetical performance values obtainable if there were no spatial modulation on the beam. Separation between these curves is a measure of peak to average spatial modulation.

11) Calculated output power and energy for the Nova baseline laser system. The curve labeled "performance" corresponds to calculated values obtained when "B" damage fluence limitations are imposed. The curve labeled "B" corresponds to hypothetical performance values obtainable if there were no spatial modulation on the beam. Separation between these curves is a measure of peak to average spatial modulation.

12) Calculated output power and energy for the Nova baseline laser system. The curve labeled "performance" corresponds to calculated values obtained when "C" damage fluence limitations are imposed. The curve labeled "C" corresponds to hypothetical performance values obtainable if there were no spatial modulation on the beam. Separation between these curves is a measure of peak to average spatial modulation.

13) Calculated power performance of the Nova baseline laser chain. The upper two curves correspond to values obtained when "A" and "B" fluence limits for optical damage are imposed. The bottom curve corresponds to performance limits imposed by nonlinear phase retardation and concomitant growth of spatial instabilities (B-limit). A B-limit of 3.5 radians for the incremental phase retardation accumulated between each pair of spatial filters has been imposed on the calculations leading to the bottom curve.

13A) Calculated fluence values along the Nova Phase I chain for 3 ns pulses. The solid curves represent peak values of the modulated beam fluence; the

upper curve reproduces Figure 7, while the lower curve includes the effects of gain saturation in a realistic model. Average fluence at each lens is designated by the symbol M.

14) Calculated values of amplified spontaneous emission from Nova. Calculations assume "B" fluence limited performance at 3 ns. Further assumptions include a 30:1 contrast ratio for the 10 cm Pockels' cell, 50 ns gate widths for all Pockels' cells, and a 300 μsec (FWHM) width of the amplified fluoresence pulse at the output of the amplifier chain.

15) Calculated time evolution of amplified spontaneous emission (ASE) energy density and total ASE energy for a single Nova amplifier chain. Energy density is calculated at a plane 1 mm forward of best focus for the f/3 final focusing lens. In region I all Pockels' cells are closed. In region II the P.C.'s are open but the main laser pulse has not yet arrived at the target. In region III the P.C.'s remain open but target irradiation is completed.

16) Calculated ASE power distribution from a single Nova chain at the focal plane of the final f/3 target focusing lens. For these calculations, all Pockels' cells remain closed. The rectangular step-like distribution arises from the superposition of individual, uniformly illuminated, spatial filter pinholes.

17) Final focusing geometry and calculated intensity at best focus for the ten-beam Nova Phase I baseline laser.

FILTER/RELAY	F-NUMBER	PINHOLE DIAM. (mm)	ANGULAR ACCEPTANCE APERTURE (μrad)*
460 mm / 740 mm	20	3.3	360
315 mm / 460 mm	20	1.5	340
208 mm / 315 mm	25	1.0	190
146 mm / 208 mm	20	0.75	250
92 mm / 146 mm	11	0.3	300
92 mm / 92 mm	11	0.3	300
42 mm / 92 mm	18	0.76	1000
27 mm / 42 mm+	66	1.3	730

Table 1: NOVA CHAIN SPATIAL FILTER/RELAY PARAMETERS

*Full Angle

+This relay is not shown in Figures 1 and 2. It follows the apodizing chain input aperture.

Fluorophosphate	Vendor	λ(μm)	$\sigma_{(pm^2)}$	τ(μs)	$\Delta\lambda$(nm)	n_o	n_2 (10^{-13}esu)	E_s(1 ns)
LGH-10	Hoya	1.051	2.6	475	31.3	1.45	0.58	4.9
E-309	O.I.	1.051	2.5	510	31.3	1.43	0.54	5.1
LG-810	Schott	1.051	2.6	495	31	1.43	0.49	5.1
ED-2 Silicate	O.I.	1.064	2.7	359	34.4	1.56	1.41	4.5

Table 2

PROPERTIES OF FLUOROPHOSPHATE AMPLIFIER GLASSES

Attenuation (cm^{-1})		Homogeneity		Damage† Fluence (J/cm^2)	
Min	Goal	Min	Goal	Min	Goal
≤ 0.002	≤ 0.0015	$\pm 1.5 \times 10^{-6}$	$\pm 1 \times 10^{-6}$	≥ 23	≥ 35

Table 3
CRITERIA AND SPECIFICATIONS FOR NOVA GLASS AMPLIFIER DISKS

†Measured normal to beam in air. Actual fluence in a (tilted) disk is reduced by the index of refraction n_0.

NOVA CHAIN DESIGN

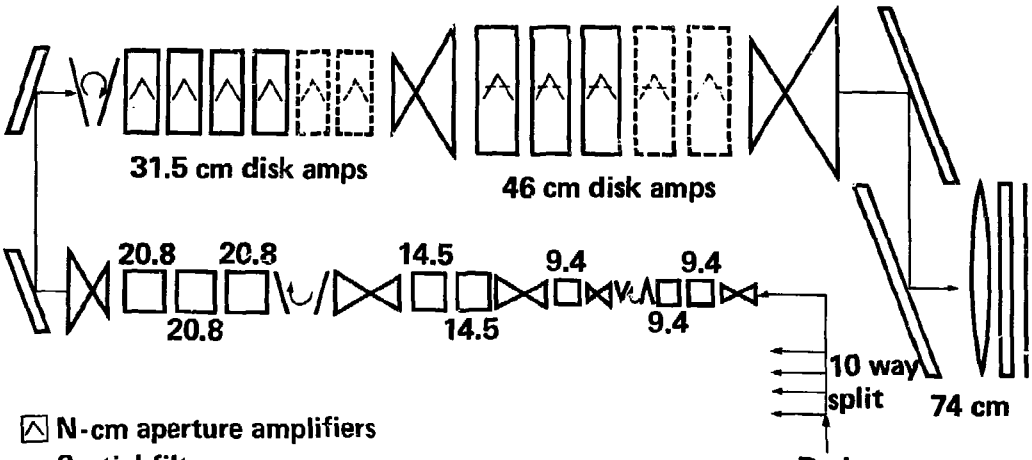

02-31-0180-0047

Figure 1

PROPAGATION GEOMETRY FOR HIGH POWER LASER CHAINS

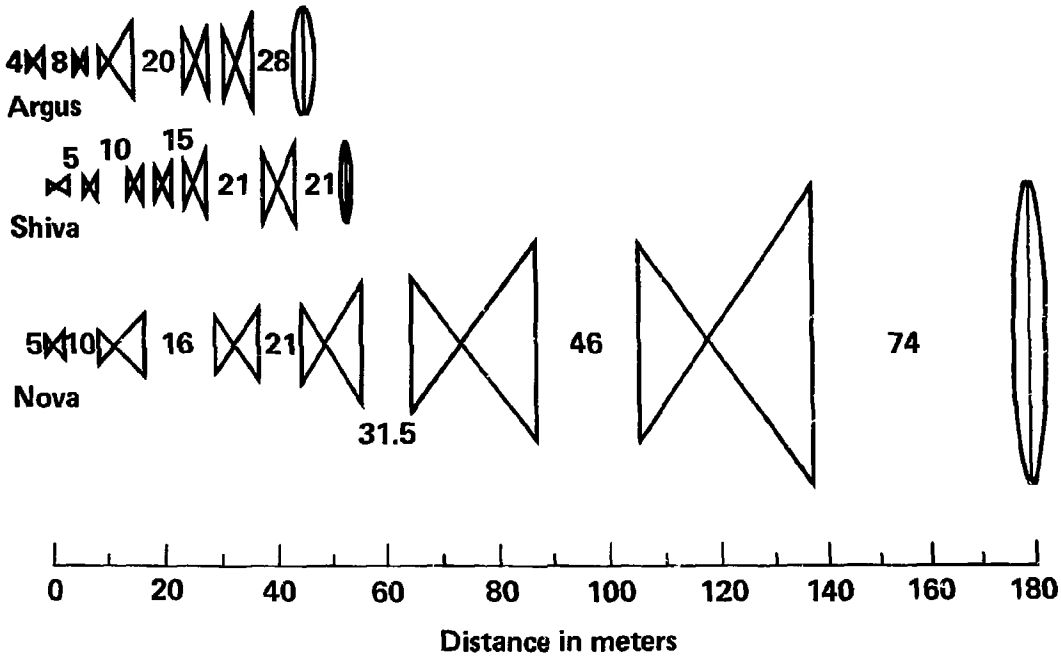

02-90-0180-0048

Figure 2

NOVA DESIGN FLUENCE LEVELS (J/cm^2)

	Antireflection			Uncoated		
	100 ps	1 ns	3 ns	100 ps	1 ns	3 ns
"A"	1.6^{*}	5^{*}	5.5^{*}	5.1^{*}	16^{*}	28^{*}
"B"	2.5^{**}	8^{**}	8.5^{**}	6^{**}	19^{**}	33^{**}
"C"	3.8^{++}	12^{++}	12.5^{++}	11^{+++}	35^{+++}	61^{+++}

* Median damage threshold for today's surfaces

** Damage threshold for best of today's surfaces

++ Super polish

+++ Laser polish/graded index

02-31-0180-0046

Figure 3

MEASURED SATURATION FLUX OF E-309 FLUOROPHOSPHATE

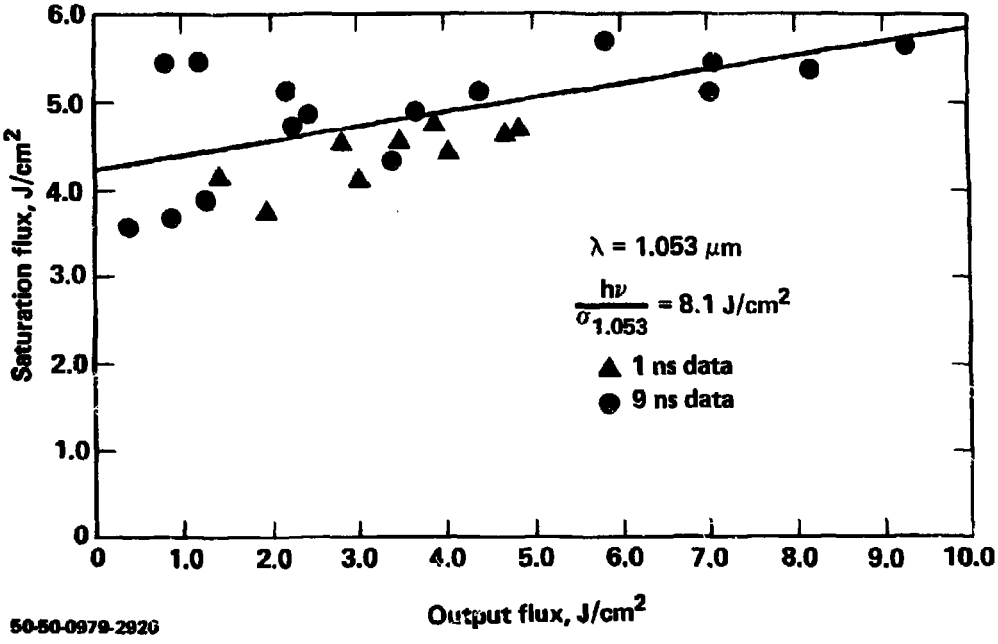

Figure 4

FLUOROPHOSPHATE AMPLIFIER DESIGNS

Clear aperture	315 mm	460 mm
Thickness	49 mm	38 mm
Disks per module	2	2
SS gain per module	1.65	1.65
Gain coeff.	4.3/m	5.4/m
Energy density	300 J/L	400 J/L
Glass volume per module	15 L	24 L
Bank energy per module	300 kJ	800 kJ
αD	2.5	2.5

02-50-0180-0130

Figure 5

NOVA CHAIN PERFORMANCE

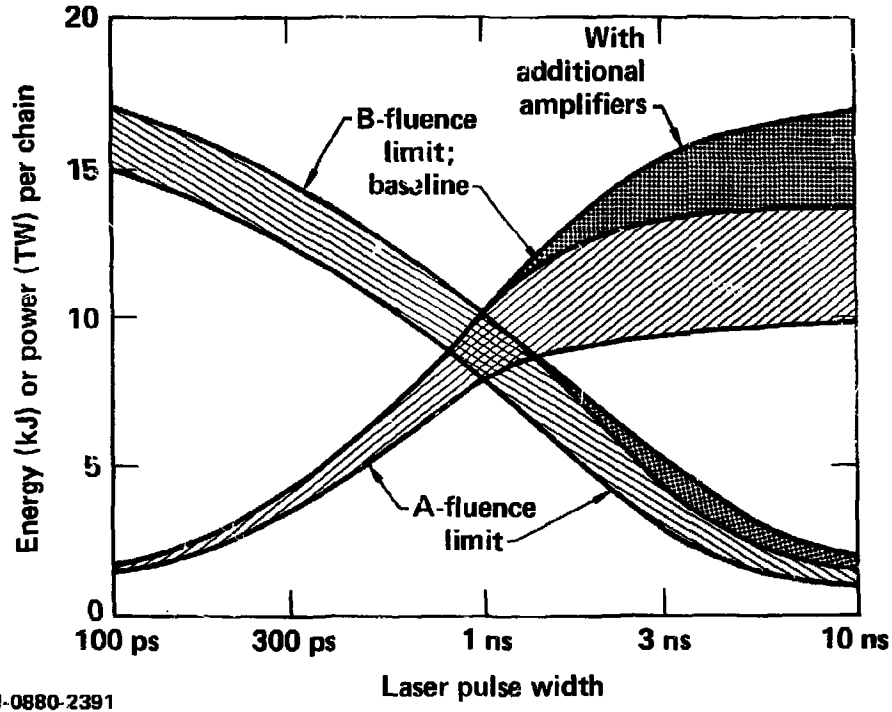

02-31-0880-2391

Figure 6

FLUENCE LEVELS ALONG THE NOVA CHAIN

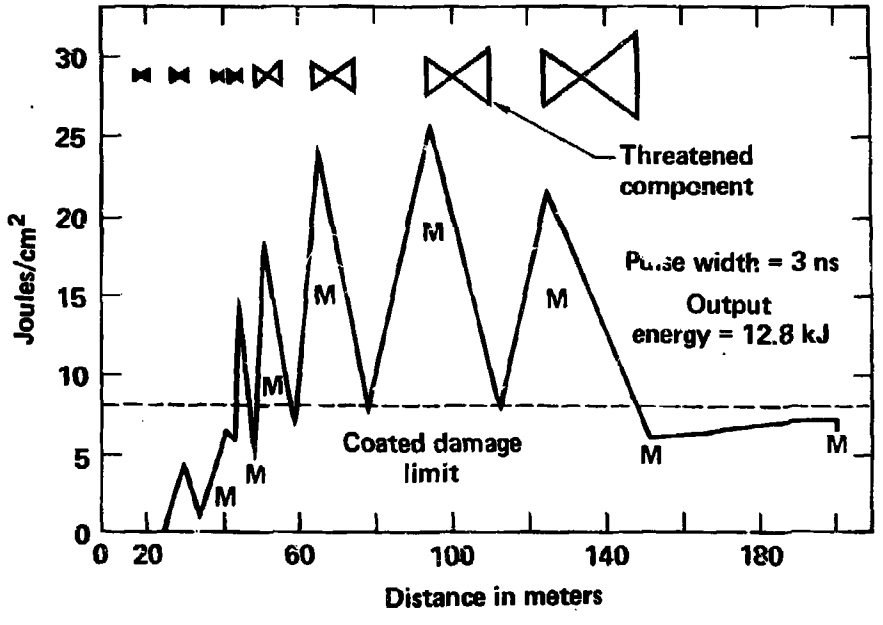

02-31-0180-0044

Figure 7

NOVA CHAIN PERFORMANCE

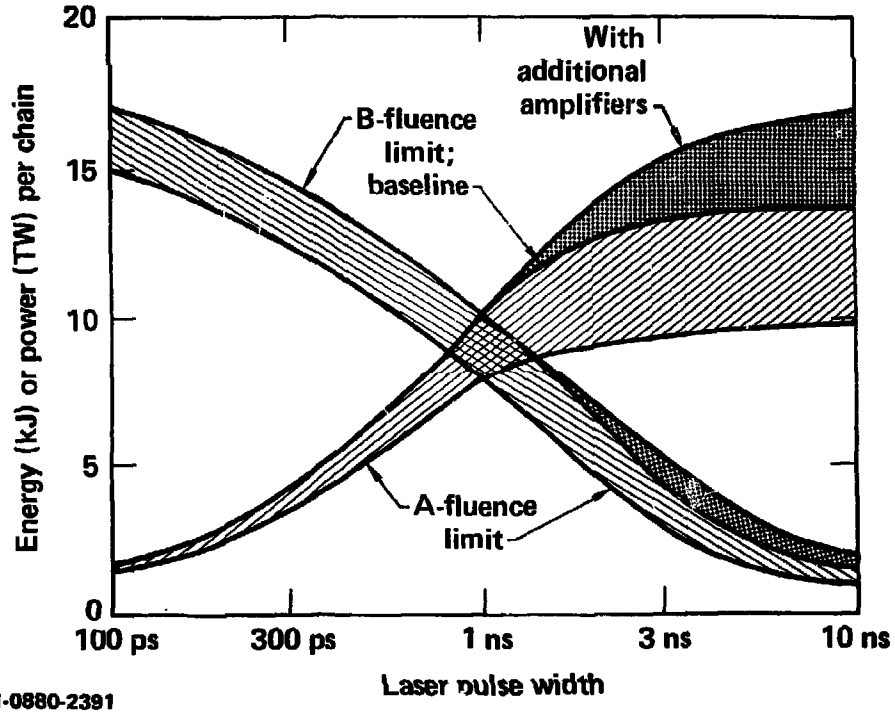

02-31-0880-2391

Figure 6

FLUENCE LEVELS ALONG THE NOVA CHAIN

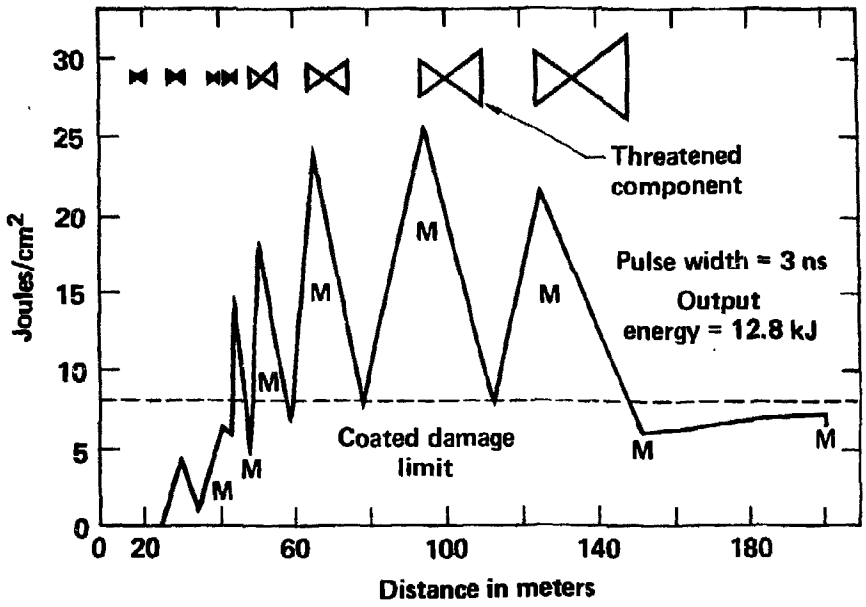

02-31-0180-0044

Figure 7

FLUENCE LEVELS ALONG THE NOVA CHAIN

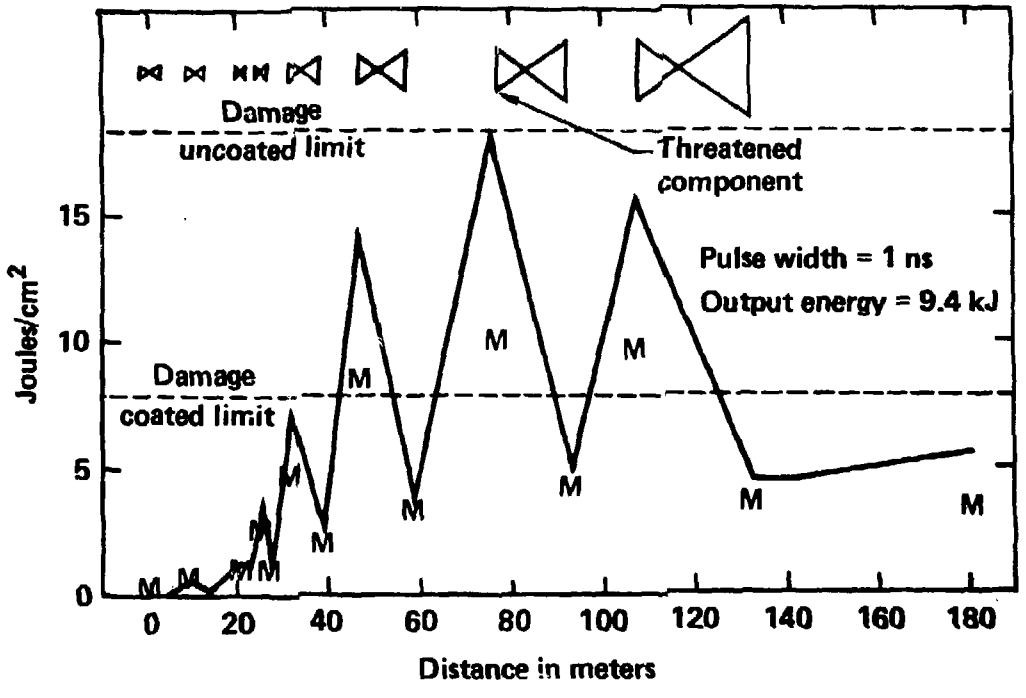

02-31-0180-0127

Figure 8

FLUENCE LEVELS ALONG THE NOVA CHAIN

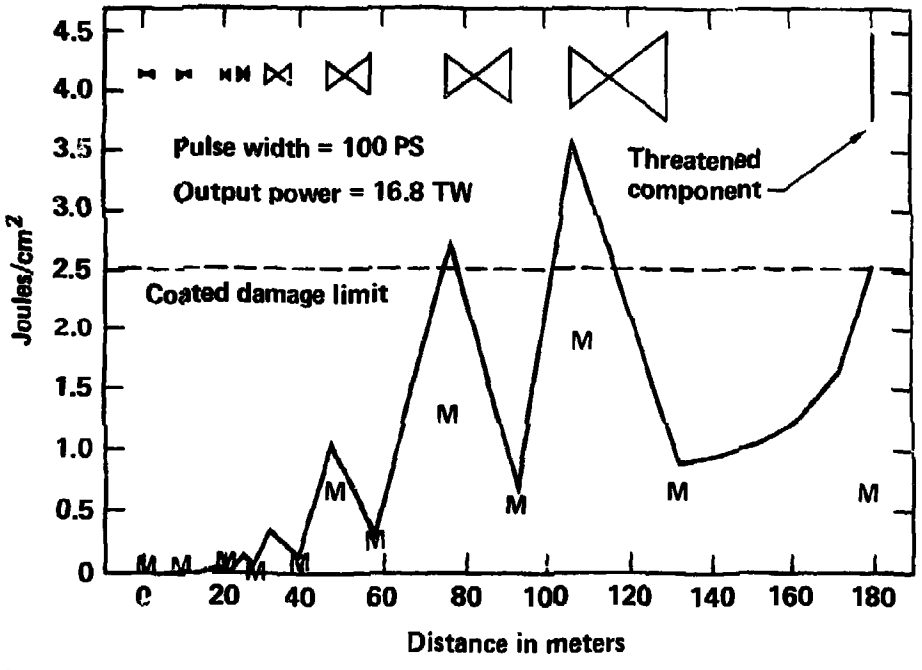

02-31-0180-0128

Figure 9

"A" FLUENCE LIMITATIONS ON NOVA CHAIN

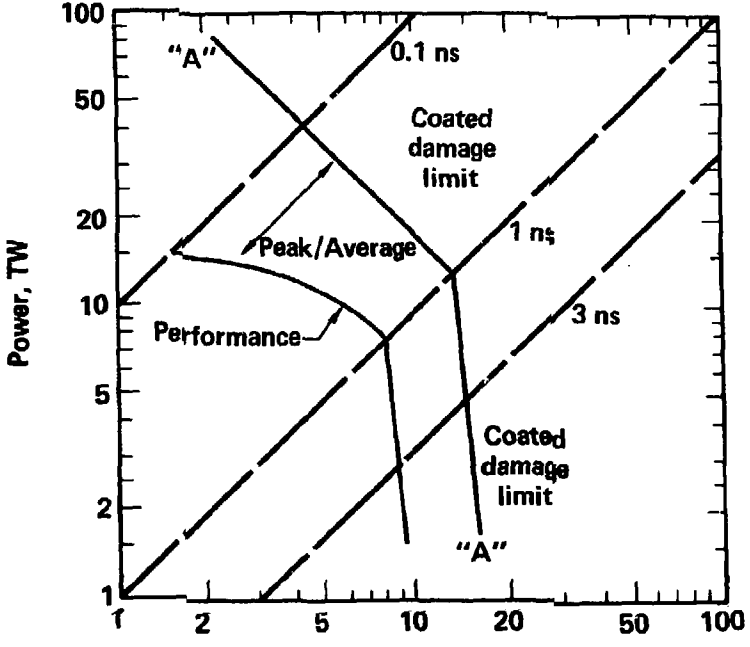

02-31-0180-0041

Figure 10

"3" FLUENCE LIMITATIONS ON NOVA CHAIN

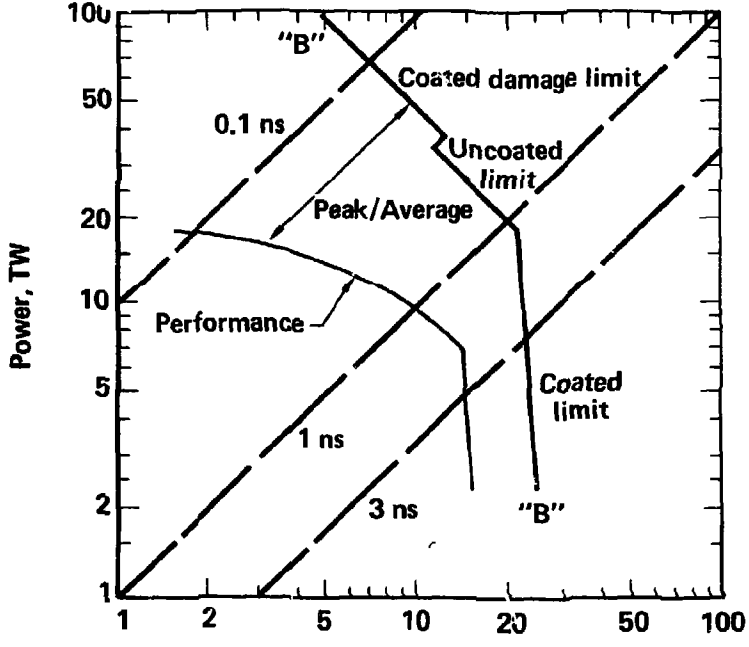

02-31-0180-0043

Figure 11

"C" FLUENCE LIMITATIONS ON NOVA CHAIN

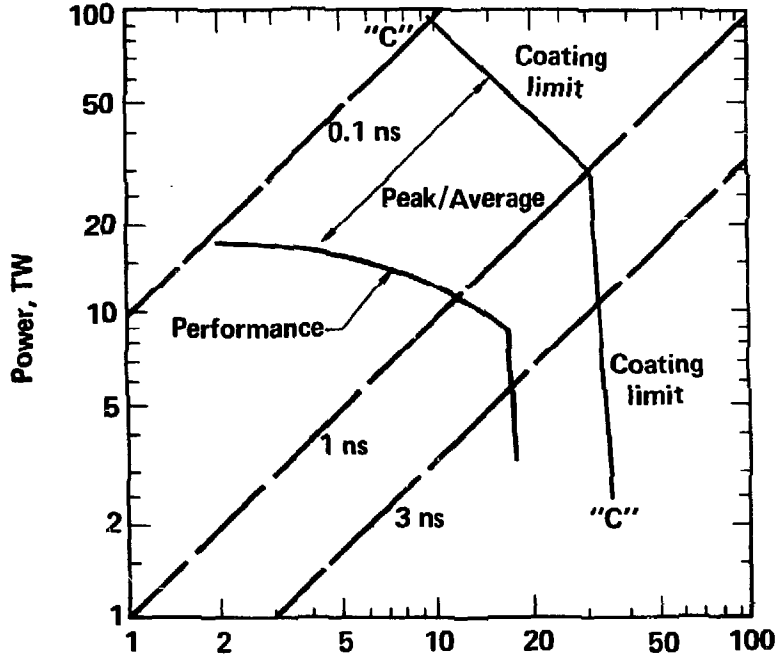

02-31-0180-0042

Figure 12

NOVA SINGLE CHAIN POWER PERFORMANCE

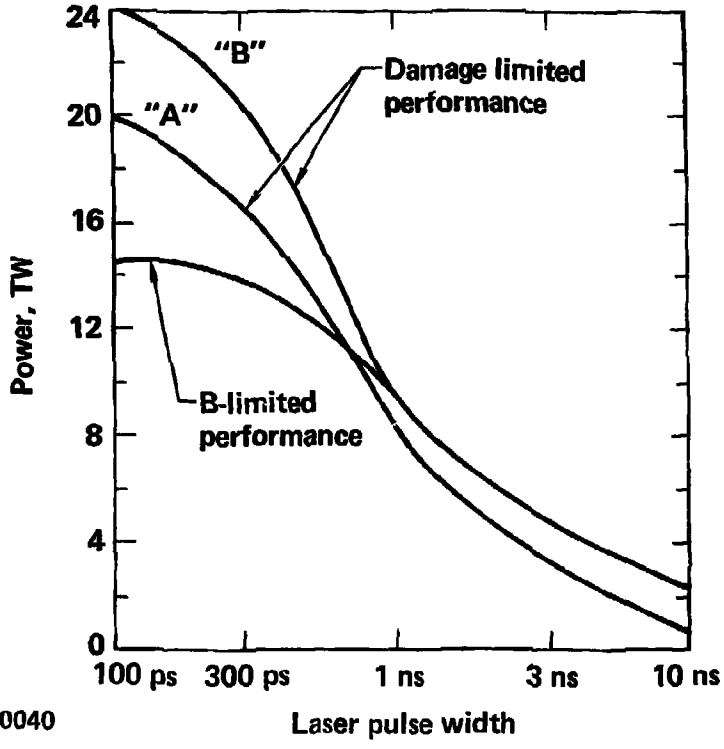

02-31-0180-0040

Figure 13

FLUENCE LEVELS ALONG NOVA CHAIN

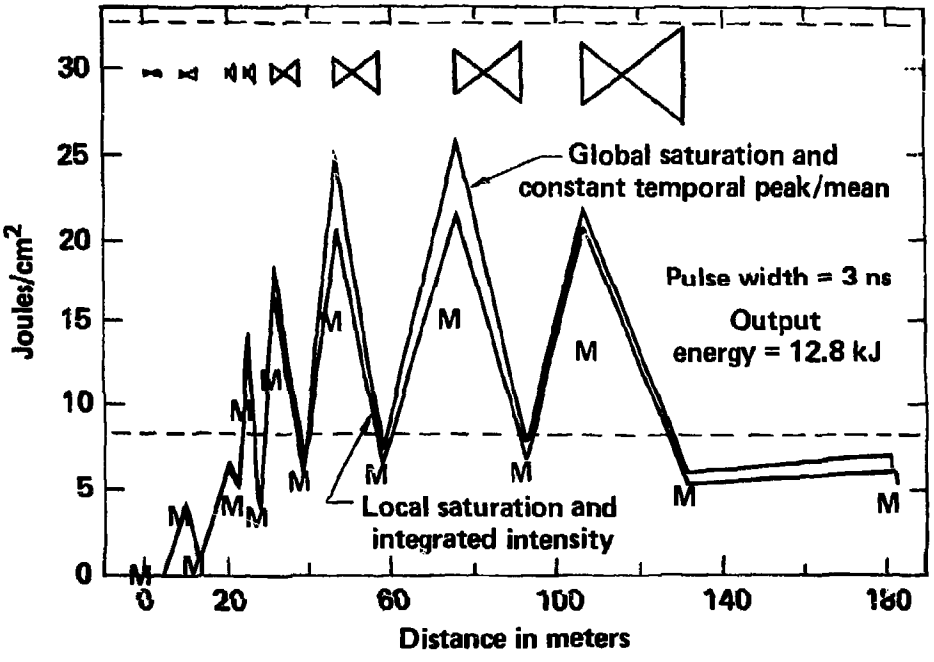

02-31-0380-1033

Figure 13A

NOVA ASE PER CHAIN

	Pockels cells closed		All pockels cells open (50 ns gate without 10 cm PC)
	Without 10 cm pockels cells	With 10 cm pockels cells	
ASE energy per beam	5 mJ	550 μJ	24 mJ
Peak energy density in focal plane	84 J/cm^2	7.7 J/cm^2	(2.5)10^4 J/cm^{2*}
Peak energy density 1 mm from focal plane	5.3 J/cm^2	0.48 J/cm^2	28 J/cm^2
Peak power density in focal plane	(2.8)10^5 W/cm^2	(2.6)10^4 W/cm^2	(5) 10^{11} W/cm^{2*}
Peak power density 1 mm from focal plane	(1.8)10^4 W/cm^2	(1.6)10^3 W/cm^2	(2.6)10^8 W/cm^2

B-Fluence 3 ns level drive
30:1 contrast for 10 cm pockels cells
50 ns gate for all pockels cells
300 μs (FWHM) fluorescence pulse

*diffraction limited spot

02-01-0180-0124

Figure 14

PREDICTED NOVA ASE

(1 mm From Focal Plane of f/3 Lens)

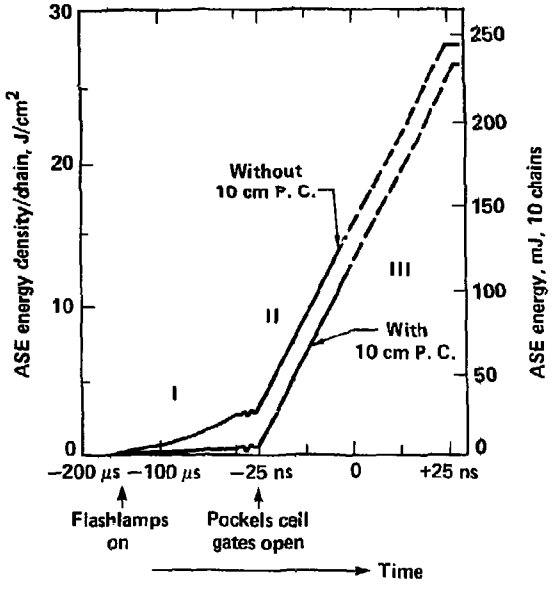

Assumptions

- B-fluence, 3 ns drive
- 300 μs (FWHM) fluorescence pulse
- 50 ns pockels cell gate

Figure 15

02-31-0180-0125

NOVA ASE POWER DISTRIBUTION AT FOCAL PLANE OF f/3 TARGET LENS

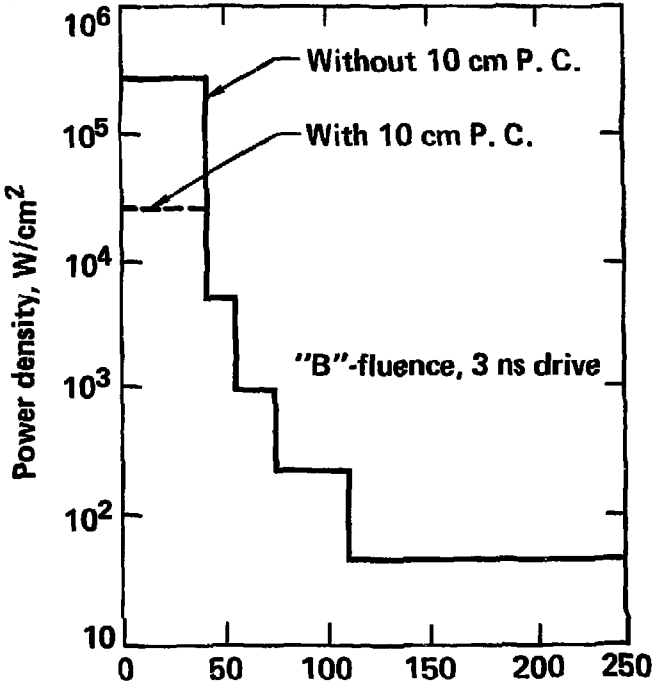

02-31-0180-0126

Figure 16

ESTIMATED NOVA ϕI INTENSITY DISTRIBUTION AT 1 NS

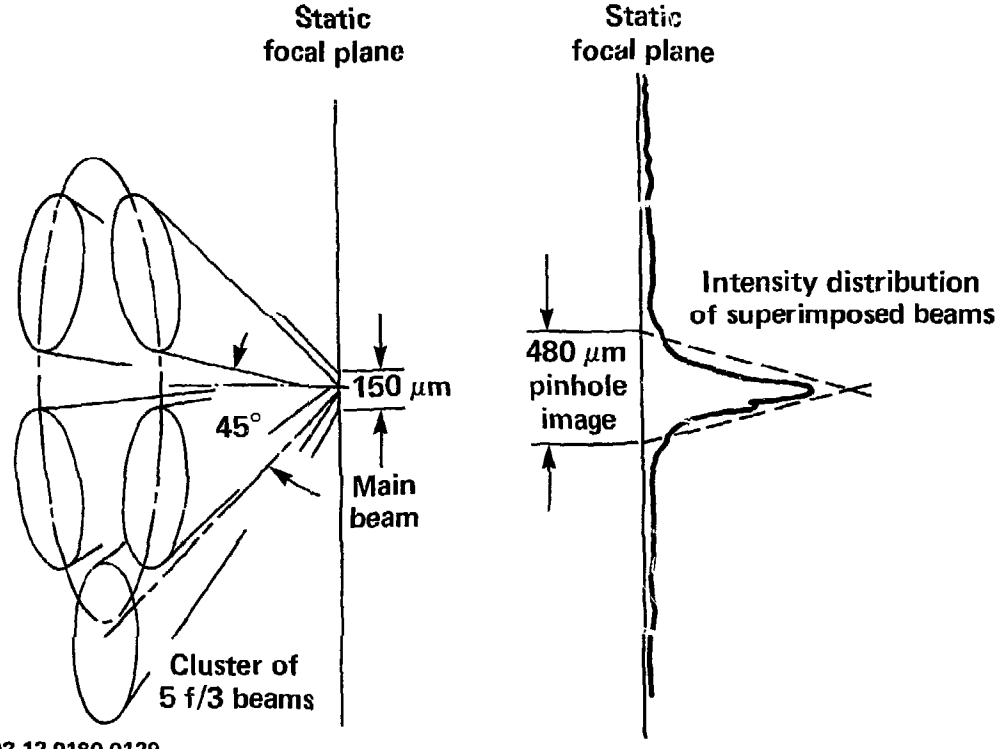

02-12-0180-0129

Figure 17